Highly stable subnanometric Pt clusters in all silica K-doped zeolites: implications for the CO oxidation reaction

Benjamin Bohigues, Isabel Millet, Patricia Concepción, Avelino Corma, Manuel Moliner, Pedro Serna**

Instituto de Tecnología Química, Universitat Politècnica de València-Consejo Superior de Investigaciones Científicas, Avenida de los Naranjos s/n, 46022 València, Spain

*Corresponding authors: mmoliner@itq.upv.es, psername@itq.upv.es

Abstract: Small metal clusters can provide improved catalytic activity compared to single metal atoms and larger metal nanoparticles of the same element. The stabilization of metal ensembles of a few atoms is extremely challenging, however, because reductive sintering and oxidative fragmentation are phenomena that often occur at low temperatures in reactive atmospheres. In this regard, the CO oxidation reaction is particularly challenging, because CO tends to aggregate noble metals on non-reducible supports, such as SiO_2, whereas O_2 triggers the formation of (less active) single atoms on reducible supports, such as CeO_2. Accordingly, state-of-the-art Pt/CeO_2 catalysts undergo severe deactivation under practical CO oxidation conditions in excess of O_2. In this contribution, we report a highly active CO oxidation catalyst that is able to overcome both sintering and fragmentation instabilities under conditions that make other alternatives to fail. The catalyst is based on small Pt clusters inside K-MFI, that benefits from both strong metal/support interactions at defective sites of the zeolite, and strong electronic promotion by the support, to attain highly stable, highly active, electron-rich Pt clusters.

Keywords: Pt cluster, electronic promotion, CO oxidation, stability and oxidative conditions

TOC Graphic

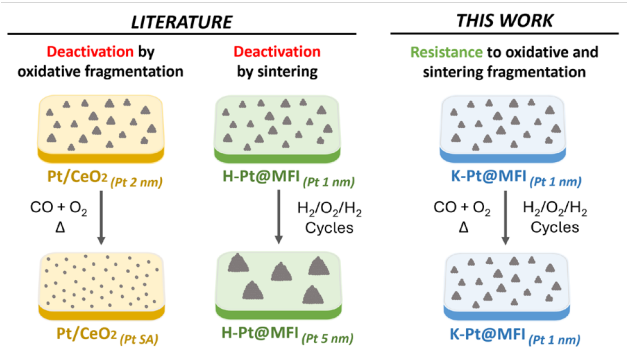
LITERATURE
THIS WORK
Deactivation by oxidative fragmentation
Deactivation by sintering
Resistance to oxidative and sintering fragmentation
Pt/CeO2 (Pt 2 nm)
H-Pt@MFI (Pt 1 nm)
K-Pt@MFI (Pt 1 nm)
CO + O2
Δ
H2/O2/H2 Cycles
CO + O2
Δ
H2/O2/H2 Cycles
Pt/CeO2 (Pt SA)
H-Pt@MFI (Pt 5 nm)
K-Pt@MFI (Pt 1 nm)

Introduction

Supported Pt catalysts have been intensively studied to convert carbon monoxide (CO) to carbon dioxide (CO_2) via oxidation and water-gas-shift (WGS) reactions as elemental steps in industrially-relevant applications, such as vehicle emissions control [1–3] or CO removal in fuel cells.[4,5]

Pt clusters and small nanoparticles are highly active species for the CO oxidation reaction, as they show effective to activate both CO and O_2 at moderate temperatures in mixtures of the two reactants.[3,6–9] Pt on ceria, in particular, has received wide attention in the last years,[9–11] thanks to the participation of the support as a redox active material than can a) participated in the reaction as a co-catalyst; and b) promote strong metal support interactions (SMSI).[11–13] It is believed that surface oxygen vacancies on ceria can activate O_2 readily, allowing a concerted activation mechanism between CO adsorbed on the Pt, and O_2 activated at the metal-support interface, that offers superior CO oxidation performance.[7] These promoting effects are usually more pronounced when Pt is in the form of single atoms rather than metal nanoparticles,[11] because the former maximize the interaction with the support. However, the lack of neighboring Pt-Pt bonds in single atom Pt/CeO_2 catalysts overrides key cooperativity that also occurs between Pt atoms in small clusters and nanoparticles,[14] which reveals necessary to achieve optimal performance. Accordingly, small Pt nanoparticles on CeO_2 are more active than isolated Pt atoms on this support.[15]

An important limitation of Pt/CeO_2 catalysts for the CO oxidation reaction is that state-of-the-art materials consisting of small metal nanoparticles deactivate fast in O_2-rich atmospheres at moderate-to-high temperatures (conditions relevant to automotive

applications, for example), following an oxidative fragmentation process that yields (less active) Pt atoms strongly trapped by the support via SMSI.[11,13]

On the other hand, typical non-reducible supports interact with metals too weakly to stabilize the most dispersed forms of the active sites when the reaction conditions are harsh (e.g. high temperature in the presence of reducing or oxidizing gases).[16] Non-reducible supports, moreover, lack redox functionality and, thus, cannot replicate the cooperative role of CeO_2 in CO oxidation catalysis.

Certain non-reducible supports, such as zeolites, can nonetheless be precisely designed to a) influence metals via electronic promotion and acid/base cooperation;[14] and b) enhance the stability of various types of metal species within their well-defined pores and cavities, including single atoms, subnanometric clusters and nanoparticles.[17–19] One advantage of zeolites compared to other common solid supports is, indeed, that the chemical environment of metals inside their micropores is highly tunable, following rules that can be, to a large extent, rationalized (for example, in terms of extra-framework charge compensation).[16,20,21] In the last decade, significant progress has been made to develop noble metal catalysts with outstanding stability in various atmospheres that include O_2, H_2, CO, and H_2O. For example, Al-rich zeolites (Si/Al<10) have been shown efficient solid traps of single Pt atoms formed under oxidative atmospheres at high T,[16,22,23] thanks to the stabilizing role of Al-pairs to accommodate dicationic extra-framework species.[22,24,25] Similar to CeO_2-supported Pt catalysts, the deactivation of metallic Pt clusters by oxidative fragmentation in O_2 has been observed using Pt/CHA zeolites in the methane combustion reaction.[19] Under CO oxidation conditions, however, this zeolite yields metallic Pt nanoparticles, even if the reaction is run in excess of O_2,[19] whereas Pt in CeO_2-supported systems undergoes re-dispersion into single metal atoms.[13] Although

the Pt/CHA zeolite avoids deactivation by oxidative fragmentation into single Pt atoms, the activity of this system, expressed as a TOF (on a per total Pt basis) is modest.

Recently, we developed a new K-Pt@MFI catalyst with outstanding redox stability. In this system, the presence of K has been proven to enhance the stability of single Pt atoms under conditions that favour Ostwald-ripening sintering (e.g. in O_2 at high temperature) on other supports, at the time that the stability of subnanometric Pt clusters in reducing atmospheres (e.g. in H_2) is also enhanced. As a result, the massive metal agglomeration otherwise observed when non-reducible supports are subjected to severe redox stress, is strongly hindered.[26] It has been postulated that particular framework defects (i.e. silanol/siloxy nests) that form at the sinusoidal channels of MFI when synthesized in the presence of K, with no Al present, are the key to stabilize so small Pt clusters under such harsh reaction conditions.[27–29] The exact nature of these anchoring sites remains, however, unresolved.

An underlying premise of the present work is that the Pt speciation in K-Pt@MFI, under CO oxidation conditions, shares certain similarities with the Pt@Al-MFI system, particularly, the fact that oxidative fragmentation paths that turn metallic Pt clusters into single Pt atoms are attenuated, opening the door to improvements over incumbent Pt/CeO_2 technology. This result would be particularly relevant if, moreover, the K-doped catalyst manifested significant electron-promotion of the Pt species, as previously reported, and the overall catalyst redox stability was improved relative to these previous precedents.[30–32] Keeping these incentives in mind, we decided to investigate the behaviour of the one-pot synthesized K-Pt@MFI [26,33] for the CO oxidation reaction.

Materials and Methods

Synthesis of Pt-Containing Zeolites

One-Pot Synthesis of $K_{0.6}$-Pt@MFI. Firstly, 10.25 g of tetrapropylammonium hydroxide solution (40 wt.% TPAOH, from Alfa-Aesar without K traces, product code: 17456.22) was mixed with 10 g of distilled water, 17.36 g of tetraethyl orthosilicate (TEOS) and 300 mg of 20 wt.% KCl solution. The resultant solution was stirred for 3 h at room temperature to hydrolyze the TEOS. Meanwhile, another solution was prepared mixing 0.021 g of chloroplatinic acid with 9 g of distilled water and 1 g of ethylenediamine, and the resultant solution was kept under stirring for 2 h to form the corresponding complex. Then, the platinum complex solution was added to the above mixture and kept under stirring overnight. The resultant yellow mixture was transferred to Teflon-lined autoclaves and heated in an electric oven at 175˚C for 96 h under static conditions. After the hydrothermal synthesis, the solid product was filtrated and washed with distilled water and acetone and dried at 60˚C. The solid sample was calcined under air flow at 600˚C during 4 h with a ramp of 2˚C/min to obtain the calcined form of the K_x-Pt@MFI (x represents the K wt.% in the final sample). The amounts of Pt and K in the final product were ~0.2 wt% and ~0.6 wt%, respectively. The final formation of well encapsulated Pt nanoclusters within MFI, $K_{0.6}$-Pt@MFI, was achieved after reducing the calcined sample with a H_2 flow at 600˚C for 2 h with a ramp of 10˚C/min.

One-Pot Synthesis of $K_{0.3}$-Pt@MFI. The synthesis procedure is the same than the one described above for $K_{0.6}$-Pt@MFI, but adjusting the amount of KCl introduced (150 mg of a 20 wt.% KCl solution).

Synthesis of K_0-Pt@MFI. To extract the K while maintaining the Pt content, the calcined $K_{0.6}$-Pt@MFI was exposed to an acidic ion-exchange treatment. In particular, 0.5 g of the

calcined $K_{0.6}$-Pt@MFI was added to a previously prepared acid mixture between 1 ml of HNO_3 69% and 3 mL of HCl 37%, and the resultant mixture was maintained under stirring for 5 min at room temperature. Afterwards, the mixture was filtrated and washed with abundant distilled water until reaching a neutral pH in the wastewater. The formation of the Pt nanoclusters was achieved following the same reduction treatment with H_2 at 600°C described previously for the $K_{0.6}$-Pt@MFI.

Synthesis of H-Pt@MFI. Platinum was incorporated into a commercial MFI using an aqueous ion exchange procedure as follows: 1 g of a commercially-available MFI in its NH_4^+ form (CBV3024, Zeolyst, Si/Al~15) was mixed with a solution of 4 mg of $Pt(NH_3)_4(NO_3)_2$ (Sigma Aldrich, 99.995%) and 10 g of distilled water. The resultant mixture was kept under stirring overnight and, then, filtrated and washed with distilled water to obtain the H-Pt@MFI containing a ~0.2 wt.% Pt. The final sample was exposed to the same calcination and reduction treatments described before.

Synthesis of Pt/CeO₂. This material has been prepared by incipient wetness impregnation as follows: 76 mg of an aqueous solution of chloroplatinic acid (8 wt.%) was added dropwise to 3 g of nanosized CeO_2 (Rhodia). The resultant wetness impregnated solid was dried at 100°C for 2 h and, the final Pt/CeO_2 sample with 0.2 wt.% Pt was calcined at 450°C (ramp of 5°C/min) for 5 h in flowing air to obtain a high Pt dispersion and reduced at 300°C for 40 min with 4% CO in N_2 flow.

Characterization

Powder X-ray diffraction (PXRD) measurements were performed with a multisample Philips X'Pert diffractometer equipped with a graphite monochromator, operating at 40 kV and 35 mA, and using Cu Kα radiation (λ = 0,1542 nm).

The chemical analyses were carried out in a Varian 715-ES ICP-Optical Emission spectrometer, after solid dissolution in HNO_3/HCl/HF aqueous solution.

The morphology of the samples was studied by field emission scanning electron microscopy (FESEM) using a ZEISS Ultra-55 microscope and by field emission transmission electron microscopy (TEM) using a JEM 2100F microscope.

Infrared spectra of adsorbed CO on the Pt-zeolites were recorded at room temperature with a Nexus 8700 FT infrared spectrometer using a deuterated triglycine sulphate detector acquiring at 4 cm^{-1} resolution. An infrared cell allowing in situ treatments in controlled atmospheres and temperatures from 25°C to 500°C was connected to a vacuum system with gas dosing facility. For infrared studies the samples were pressed into self-supported wafers and pretreated in H_2 (10%) flow at 350°C for 3 h followed by vacuum treatment (10^{-5} mbar). After activation the samples were cooled to 25°C under dynamic vacuum conditions followed by CO dosing at increasing pressure (0.4-8.5 mbar). Infrared spectra were recorded after each dosage of CO.

CO Oxidation Reaction Test

In a typical experiment, 100 mg of the pelletized catalyst (pellets: ~0.2-0.4 mm) was added with 0.3 g of silicon carbide (Fisher Chemical, pellets: ~0.6 mm) and loaded in a conventional tubular plug-flow reactor (ID = 9nm). The reactor was heated at 150°C with N_2 flow (50 ml/min) and, then, while maintaining the catalyst bed at 150°C, the reaction mixture was flowed at atmospheric pressure: 53 ml/min, containing 1.3 % CO, 8.2 % O_2, balanced with N_2 (O_2-rich conditions). For the experiment using Pt/CeO_2, the initial temperature was lowered until room temperature. The downstream reaction effluents were analyzed continuously by gas chromatography (GC8890, Agilent). At each

temperature point, the reaction was maintained for 30 min after observing that the CO conversion remained unaltered. The CO conversion was calculated as follows:

$$\text{CO Conversion} = \frac{1 - \text{CO}_{(\text{outlet})}}{\text{CO}_{(\text{inlet})}}$$

$$\text{TOF } (s^{-1}) = \frac{mol\ \text{CO}_{(\text{converted})}}{mol\ \text{Pt} \cdot \text{s}}$$

Results and Discussion

Electronic Promotion of Pt in Siliceous Pt@MFI Catalysts

To investigate the effect of K as an electronic modifier, we prepared one-pot K-Pt@MFI zeolites at variable K contents (0.3 and 0.6 wt.%), and maintained constant the Pt loading at 0.2 wt.%. Following reported protocols (see experimental section for synthesis details),[26] we obtained highly crystalline MFI structures ($K_{0.3}$-Pt@MFI and $K_{0.6}$-Pt@MFI, PXRD patterns in **Figure S1** in the SI), with narrow zeolite particle size distributions of ~200-300 nm (FESEM images in **Figure S2**), and chemical compositions analogous to the theoretical values introduced in the synthesis gels (**Table S1**). FESEM images showed that the abundance of large Pt aggregates on the external surface of the zeolite crystals, after consecutive calcination (in air) and reduction (in H_2) at 600°C is negligible (**Figure S2**). The homogeneous formation of ~1 nm Pt nanoparticles within the reduced $K_{0.3}$-Pt@MFI and $K_{0.6}$-Pt@MFI samples was observed by Scanning Transmission Electron Microscopy (STEM), **Figure 1 and Table S1**.[34]

To prepare comparable ~1 nm Pt clusters inside a K-free MFI, we had to develop a new synthesis protocol, because the reported one-pot method yields large Pt nanoparticles (> 5 nm) when K is not present and the organic structure directing agent (OSDA) is eliminated via calcination in air.[26] Full K removal, without neither affecting the content

of Pt or the particle size distribution of the final materials, can be instead accomplished by subjecting the parent, calcined $K_{0.6}$-Pt@MFI sample to a simple post-synthetic ion-exchange in strongly acidic conditions (see experimental section for synthesis details, and **Figure 1** for STEM images of the corresponding reduced material).

To complete this series, a commercially available acid H-MFI (Si/Al~15, CBV3024, Zeolyst) was selected as an electron-withdrawing support,[23] and was exchanged with $Pt(NH_3)_4(NO_3)_2$ to incorporate a comparable Pt loading, following well-established synthesis protocols (details in the experimental section). The resultant H-Pt@MFI sample was calcined (in air) and reduced (in H_2) at 600°C, and characterized by STEM, which revealed the formation of well-dispersed Pt nanoparticles with average sizes comparable to those in the Al-free MFI materials (i.e. ~1.1-1.2 nm, see **Figure 1**).

The textural properties of the MFI samples synthesized in this work were analyzed by N_2-BET measurements, which show that the surface areas and micropore volumes meet, in all cases, the values expected for highly crystalline MFI zeolite (**Table S2** and **Figure S3**).

IR spectroscopy was then conducted to gather information about the electronic nature of Pt in these materials, using CO as a probe molecule (CO-IR). Although it is known that the position of the CO-IR bands can be related to both geometric (e.g. particle size, such as atoms in extended terraces vs corner sites when particles are small) and electronic (i.e. electron-transfer to and from the support) effects that represent key aspects of the metal coordination environment,[14,31] the narrow difference in the Pt particle size distribution between our samples let us presume with reasonable confidence that the variability in the position of the CO bands, if observed, mainly originates from differences in the electron-density of the Pt clusters.[14,35,36] **Figure 2** shows the IR spectra of the reduced $K_{0.6}$-

Pt@MFI, $K_{0.3}$-Pt@MFI, K_0-Pt@MFI and H-Pt@MFI samples after CO-probing, revealing peaks centered around the region 2020-2080 cm^{-1}, assigned to CO linearly bonded to metallic Pt clusters in all cases.[37] In this context, blue-shift of the CO-IR bands are related to electron-transfer phenomena from the Pt to a support that acts as an electron-withdrawing macroligand, and *vice versa*. H-form, Al-containing zeolites are an example of electron-withdrawing ligands.[36] Consistent with these observations, the reduced H-Pt@MFI sample shows the greatest blue-shift in our series (band centered at ~2076 cm^{-1}), followed by the K_0-Pt@MFI sample (band centered at ~2068 cm^{-1}), followed by the $K_{0.3}$-Pt@MFI sample (three main bands at ~2068, ~2049, and ~ 2021 cm^{-1}, whose prorated average sits at ~ 2041 cm^{-1}; see details in **Figure S4**), and, finally, the $K_{0.6}$-Pt@MFI sample (band centered at ~2021 cm^{-1}), **Figure 2** and **Table S3**. These results are consistent with the role previously given to K^+ as a weak Lewis acid that increases the electron density of Pt nanoparticles upon back-donation to molecular orbitals with $2\pi^*$ character.[31] The Pt speciation that can be inferred from the CO-IR spectra of the $K_{0.3}$-Pt@MFI sample is consistent with a scenario where part of the metal is electron-enriched (band at ~ 2021 cm^{-1}) and, thus, we presume close to K^+, part is more electron-deficient (band at ~2068 cm^{-1}), as the one we observe in the K_0-Pt@MFI material, and part of the metal is in between from an electronic perspective (band at ~ 2049 cm^{-1}). Using literature references, the blue shift observed in CO-probed single noble metal atoms is ~ 40 cm^{-1} when a strong electron-withdrawing support, such as DAY zeolite, is replaced by a strong electron-donating solid, such as MgO;[38] and the shift observed with ~ 1 nm Pt clusters inside protonic forms of Al-rich HY zeolites (Si/Al = 2.5) vs the corresponding K-doped analogues can be as large as ~ 40 cm^{-1}.[31] The shift we observe in $K_{0.6}$-Pt@MFI sample vs H-Pt@MFI is ~ 55 cm^{-1}, thus, comparable to these previous examples. The low K content in the K-Pt@MFI samples is dictated by the synthesis method used to achieve

unprecedented stability of ~ 1 nm Pt clusters under severe redox stress (further discussion below).[26] This is a critical property that sharply contrasts with the low metal stability observed, typically, on non-reducible supports, where acute particle growth and, thus, deactivation, is induced under cycling H_2 and O_2 when the temperature exceeds ~ 500°C.[22,23,31]

We then evaluated the CO oxidation performance of the reduced K_0-Pt@MFI, $K_{0.3}$-Pt@MFI, $K_{0.6}$-Pt@MFI and H-Pt@MFI through light-off activity experiments at increasing temperatures. We performed reactions under O_2-rich conditions (O_2/CO= 6.3), because these are most challenging with state-of-the-art Pt/CeO_2 catalysts,[11,13] and are industrially relevant in processes such as exhaust abatement catalysis.[1,2] Activity, measured as the TOF at 200 ^{0}C (see **Figure 3a**), follows the order $K_{0.6}$-Pt@MFI > $K_{0.3}$-Pt@MFI > K_0-Pt@MFI > H-Pt@MFI. This trend correlates well with the trend observed by CO-IR (**Figure 2, Figure 3b** and **Table S3**), confirming that the CO oxidation activity of Pt clusters increases as the metal electron-density increases via support-to-metal charge transfer.[31] Moreover, whereas the $K_{0.6}$-Pt@MFI sample retains structural integrity at high temperature in CO, H_2 and O_2, drastic deactivation by metal sintering is observed with low Si/Al ratio zeolites, as demonstrated in subsequent experiments.

Particle Size Effects and Stability Against Oxidative Fragmentation

Although light-off conversion vs temperature experiments are a convenient (rapid) method to evaluate the activity of solid catalysts in fix bed reactors, they fail to inform about signs of early changes in the structure of the active sites along the conversion/temperature curve. Transient (activating or deactivating) behaviour,[19,39] are common phenomena in supported metal catalysts, more so, when the active sites present low atomicity (~ 1 nm or less). The onset activity temperature can be even greater than

the temperature required to trigger the structural change, in which case the reactivity test informs about the performance of an unknown (uncharacterized) active site.[19] Fortunately, standard lab-scale protocols can be still put in place to interrogate the consistency of the inferred structure-performance correlation, as discussed next.

These considerations are particularly relevant for the CO oxidation reaction, because additional experiments we collected on catalysts with different Pt particle size indicate that the metal nuclearity, in addition to the metal electronics, influence the catalytic activity notably, in a rather narrow size range, consistent with previous reports.[40] For example, by reducing the K_0-Pt@MFI sample, relatively neutral in terms of electron-donating/electron-withdrawing characteristics, at 200°C instead of 600°C, Pt clusters smaller than < 0.9 nm are formed,[41] as shown by STEM in **Figure S5**. This decrease in the average particle size from 1.1 nm, when reduced at 600°C, to < 0.9 nm, when reduced at 200°C, causes the light-off CO combustion curve to shift ~30°C at 50 % CO conversion (**Figure S6** in the SI). The magnitude of this drop is comparable to the drop observed by fine-tuning of the metal electron-density with K at a constant average metal nanoparticle size of ~1.1-1.2 nm (**Figure 3**). Signs of catalyst instability are evident in the K_0-Pt@MFI material reduced at 200°C, as it undergoes substantial catalytic improvement when a second light-off experiment is performed without further thermal treatment in between. This activity change is concomitant to the growth of Pt from ~ 0.9 nm diameter clusters, after the first activation in H_2 at 200°C, to ~ 1.2 nm clusters after the first reactivity test, matching very closely the cluster size of the freshly reduced K_0-Pt@MFI sample at 600°C (**Figure S7** in the SI).

In contrast to the K_0-Pt@MFI sample reduced at 200°C, the light-off curves of all 600°C reduced catalysts virtually overlap in the first and a second uses (**Figure 3**). This result is

consistent with the observation that all spent catalysts retain, in these cases, Pt within a narrow particle size range (~1.1-1.4 nm) after two consecutive light-off experiments (**Figure S8** in the SI). These results confirm that the main activity descriptor is, then, essentially electronic (**Table S3**), and confirms the suitability of non-reducible supports to limit well-known deactivation mechanisms that otherwise control the behavior of state-of-the-art Pt/CeO_2 catalysts, particularly, the oxidative fragmentation of highly active Pt nanoparticles into less active single Pt atoms when O_2 is in excess in the CO stream (e.g. as in combustion engines).[13] Thus, the $K_{0.6}$-Pt@MFI mimics previous Pt@Al-MFI zeolites to prevent this deactivation mechanism, as postulated, and triggers the formation of more active electron-rich Pt species, whose reliance to sinter under severe redox stress is also enhanced relative to the Al-containing counterpart (see additional results below).

To further test the resilience of the most active $K_{0.6}$-Pt@MFI catalyst against oxidative fragmentation, we performed new light-off experiments, and set the final reaction temperature to 500°C, as recently reported with Pt/CeO_2 catalysts.[13] Subsequently, we followed the conversion vs temperature curve through a second light-off cycle, starting at room temperature, without any additional activation treatment in between. The reduced $K_{0.6}$-Pt@MFI maintained its CO conversion profile almost unaltered at increasing temperatures for the two light-off catalysis cycles (see blue triangles in **Figure 4**), as Pt nanoparticles of virtually invariable size were also retained (STEM images, **Figures 1** and **S9** in the SI). Under identical conditions, a highly active Pt/CeO_2 catalyst made in our labs, activated in CO at 300°C prior to catalysis, underwent drastic deactivation, consistent with previous reports that demonstrate the redispersion of Pt nanoparticles into single atoms in the excess of O_2.[11,13] This oxidative fragmentation is promoted by the reducible support itself, which can readily stabilize single atoms at various types of surface defects.[11] Thus, the activity of the Pt/CeO_2 is superb in the first light-off reaction

cycle, being able to achieve full CO conversion at temperatures as low as 100°C (see orange circles in **Figure 4**), whereas the temperature needed to fully convert CO is greater than 300°C in the second light-off cycle (yellow circles in **Figure 4**). These results highlight the excellent resistance of the $K_{0.6}$-Pt@MFI against drastic deactivation that typically occurs on reducible supports, leading to superior performance under practical reaction conditions. Table S4 compares the performance of various representative catalysts in the literature for the CO oxidation reaction. At the same reaction temperature, we infer that the TOF by the $K_{0.6}$-Pt@MFI sample is at least 2 times higher than that of Pt on other non-reducible supports, and also about 2 times higher than that of Pt/CeO_2 catalysts after their exposure to O_2 (or a O_2-rich CO stream) at moderate-to-high temperatures.

High-Temperature Redox Stability

Studying the stability of catalysts at high-temperature under cycling redox stress provides valuable insights of the potential long-term suitability of catalysts for practical applications. To further evaluate the stability of materials under harsh reaction conditions, we developed a strenuous test that subjects the materials to 50 oxidation-reduction cycles at high temperature. This test far exceeds the severity of typical lab-scale tests to assert the stability of highly dispersed supported noble metals.[23]

In this protocol, we cyclically expose the catalysts to a) flowing air; b) flowing N_2; and c) flowing pure H_2; all the steps are run for 30 min at 600°C, without cooling off in between. The treatments were applied to the $K_{0.6}$-Pt@MFI, $K_{0.3}$-Pt@MFI and H-Pt@MFI samples and the aged materials were characterized by FESEM and STEM microscopies. The 50 ROR treatment was not performed to the K_0-Pt@MFI sample because previous

reports already showed that the absence of K makes the Pt sinter in this case after a single calcination in air at 600C.[26]

The formation of Pt aggregates larger than 50 nm was clearly observed in the FESEM images of the K-free H-Pt@MFI sample (**Figure S10e-f**). Accordingly, we infer that the coulombic forces present in Al-containing H-MFI supports are not sufficient to effectively hold Pt as highly dispersed clusters throughout multiple high temperature redox cycles. We note that this material shows good stability under less demanding conditions, for example, a single reduction-oxidation-reduction (ROR) cycle at 600°C, with cooling to room temperature between steps, and slow ramp up to the selected temperature.[23] These sintering issues are usually aggravated in low Si/Al zeolites, where structural degradation via dealumination is more likely to occur.[16,42] After the 50-ROR aging treatment, metal agglomeration is also observed, to a lesser extent, in the $K_{0.3}$-Pt@MFI sample (FESEM images in **Figure S10c-d in the SI**), indicating that intermediate levels of K partially prevent the undesired Pt sintering. Remarkably, FESEM images of the sample containing the higher K content, $K_{0.6}$-Pt@MFI, show negligible formation of large nanoparticles after the 50 consecutive redox treatments at 600°C (see **Figure S10a-b in the SI**). A closer inspection to this sample by STEM microscopy reveals the virtual exclusive presence of subnanometric Pt clusters inside the zeolite (see $K_{0.6}$-Pt@MFI in **Figure S11a**). The saturation of purely siliceous MFI zeolite with K appears to hinder, thus, the mobility/diffusion of otherwise highly mobile Pt species, even after exposure of the sample to strenuous conditions.

We also evaluated the aged samples directly in the CO oxidation reaction. As expected, the aged $K_{0.6}$-Pt@MFI offered the best catalytic activity in this series, showing an overwhelming 90ºC temperature drop to reach ~50% conversion of CO relative to the

next best alternative, the aged $K_{0.3}$-Pt@MFI sample (**Figure S12** in the SI). However, we were not anticipating an improvement in the activity of the aged $K_{0.6}$-Pt@MFI catalyst compared to the freshly reduced counterpart (**Figures 3 and S12** in the SI), more so after careful analysis of the Pt particle size distribution, which indicates that Pt clusters do indeed get slightly smaller after the 50 high temperature redox cycles (see discussion above on the detrimental effect of ultra-low atomicity of Pt on the CO combustion activity).

Conclusions

In this paper, we have rationalized the preparation of highly active/highly stable CO oxidation catalysts using K-MFI zeolites. The incorporation of K as a counter cation of highly defective, pure silica MFI allows to support and retain Pt clusters smaller than 1 nm under harsh reaction conditions. These highly dispersed species resist, on the one hand, oxidative fragmentation in excess of O_2 (including O_2-rich CO oxidation conditions), which causes state-of-the-art Pt/CeO_2 catalysts to deactivate; on the other hand, they also resist Ostwald-ripening sintering when exposed to severe redox stress at high temperature, in contrast to other supported catalysts based on non-reducible supports, thus, avoiding deactivation by agglomeration into low surface area metal particles. In addition to outstanding stability, a key to the high activity is the effective electron promotion of these small Pt species by K inside the MFI pores, leading to improved electron-rich metal clusters. Electronic promotion allows to compensate particle sizes effects, by which the smallest Pt clusters in some of these catalysts (< 0.9 nm) would not be so active if charge donation from the support was not substantial, as

demonstrated by a combination of microscopy, FTIR and kinetic experiments. K in our sample plays, therefore, a dual role in K-Pt@MFI samples, as a metal-electron density modifier and as a stabilization agent, resulting in an outstanding catalytic performance for the CO oxidation.

Notes

The authors declare no competing financial interest.

Acknowledgements

This work has been supported by the Spanish Government through PID2021-122755OB-I00 funded by MCIN/AEI/10.13039/501100011033 and TED2021-130739B–I00 funded by MCIN/AEI/10.13039/501100011033/EU/PRTR and by the Generalitat Valenciana by the Prometeo Program (CIPROM/2023/34). The authors are also thankful for the Severo Ochoa financial support by the Spanish Ministry of Science and Innovation (CEX2021-001230-S/funding by MCIN/AEI/10.13039/501100011033). B.B. acknowledges the Spanish Government for a Severo Ochoa FPI scholarship (PRE2022-102555). The Electron Microscopy Service of the UPV is acknowledged for their help in sample characterization.

Figure 1. STEM images of the different fresh samples after reduction in H_2 at 600°C and the corresponding particle size histogram: $K_{0.6}$-Pt@MFI (a-c), $K_{0.3}$-Pt@MFI (d-f), K_0-Pt@MFI (g-i) and H-Pt/MFI (j-l).

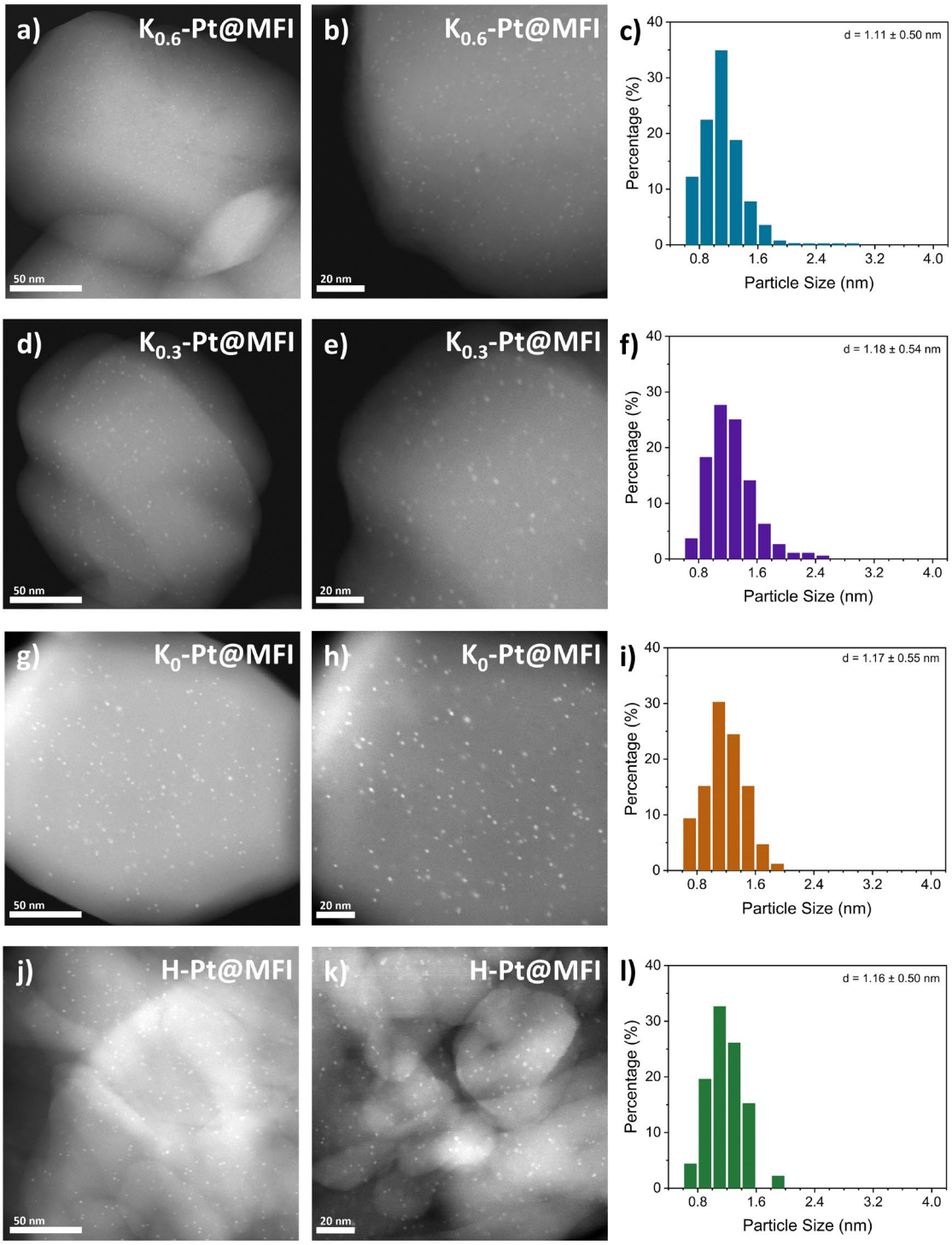

Figure 2. FTIR spectra using CO as a probe molecule at 8.5 mbar for the different Pt-containing MFI materials after sequential calcination and reduction treatments in air and hydrogen at 600°C.

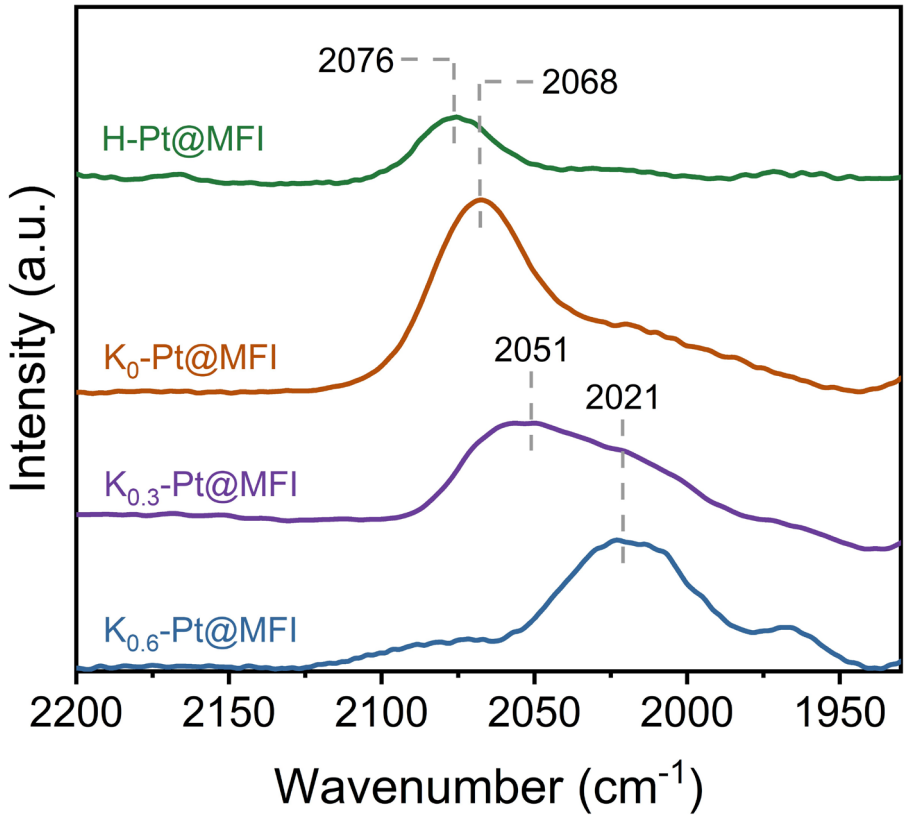

Figure 3. Catalytic activity and CO-IR spectra correlation for Pt@MFI type materials. a) CO conversion in O_2-rich conditions for $K_{0.6}$-Pt@MFI (blue), $K_{0.3}$-Pt@MFI (purple), K_0-Pt@MFI (orange) and H-Pt@MFI (green). The striped clear lines correspond to the second light-off type experiment after complete conversion for each catalyst. Reaction conditions: feed 53 ml/min (1.3 % CO, 8.2 % O_2, balanced with N_2), 100 mg catalyst, atmospheric pressure. b) Correlation between TOF for CO oxidation at 200ºC and ν_{CO} of the Pt nanoparticles from the catalysts (a lower ν_{CO} frequency indicates that the Pt nanoparticles are more electron-rich).

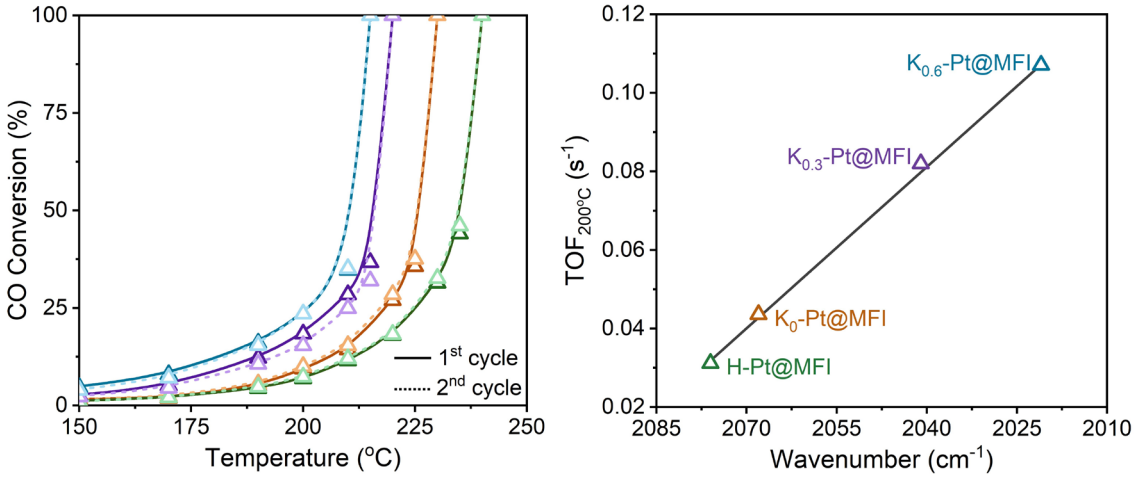

Figure 4. CO conversion in O_2-rich conditions for Pt/CeO_2 (empty orange circles) and $K_{0.6}$-Pt@MFI (empty blue triangles). The striped clear lines correspond to the second light-off cycle after reaching 500°C in the first light-off cycle for each catalyst. Reaction conditions: feed 53 ml/min (1.3 % CO, 8.2 % O_2, balanced with N_2), 100 mg catalyst, atmospheric pressure.

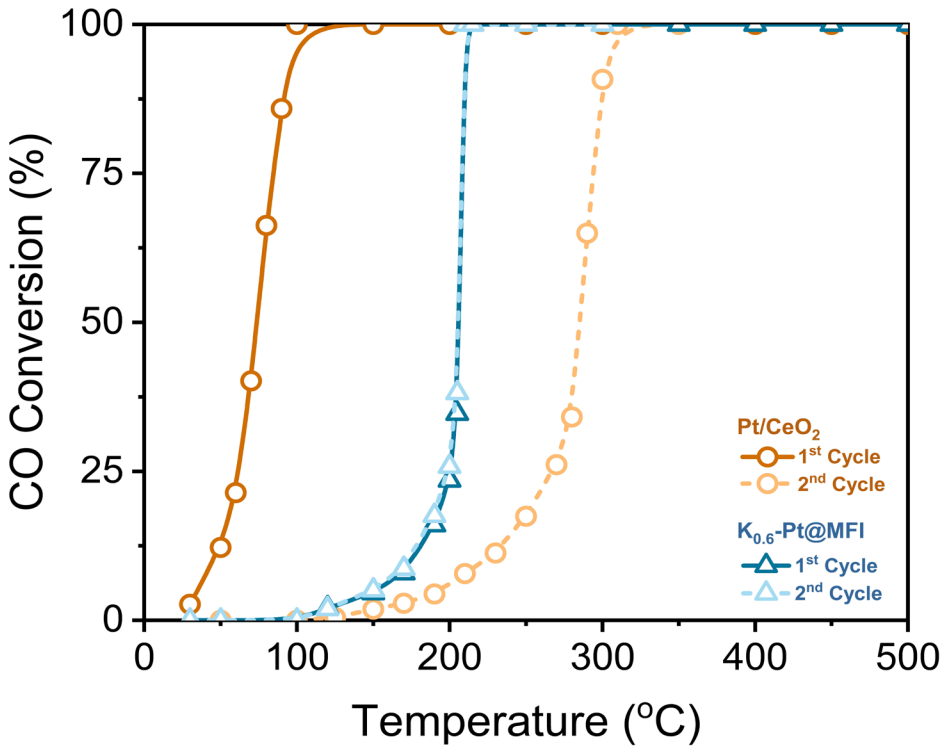

References:

(1) Kummer, J. T. Use of Noble Metals in Automobile Exhaust Catalysts. *J Phys Chem* **1986**, *90* (20), 4747–4752. https://doi.org/10.1021/j100411a008.

(2) Gandhi, H. S.; Graham, G. W.; McCabe, R. W. Automotive Exhaust Catalysis. *J Catal* **2003**, *216* (1–2), 433–442. https://doi.org/10.1016/S0021-9517(02)00067-2.

(3) Ding, K.; Gulec, A.; Johnson, A. M.; Schweitzer, N. M.; Stucky, G. D.; Marks, L. D.; Stair, P. C. Identification of Active Sites in CO Oxidation and Water-Gas Shift over Supported Pt Catalysts. *Science (1979)* **2015**, *350* (6257), 189–192. https://doi.org/10.1126/science.aac6368.

(4) Oh, S. H.; Sinkevitch, R. M. Carbon Monoxide Removal from Hydrogen-Rich Fuel Cell Feedstreams by Selective Catalytic Oxidation. *J Catal* **1993**, *142* (1), 254–262. https://doi.org/10.1006/jcat.1993.1205.

(5) Sengodan, S.; Lan, R.; Humphreys, J.; Du, D.; Xu, W.; Wang, H.; Tao, S. Advances in Reforming and Partial Oxidation of Hydrocarbons for Hydrogen Production and Fuel Cell Applications. *Renewable and Sustainable Energy Reviews* **2018**, *82*, 761–780. https://doi.org/10.1016/j.rser.2017.09.071.

(6) Wang, H.; Liu, J.-X.; Allard, L. F.; Lee, S.; Liu, J.; Li, H.; Wang, J.; Wang, J.; Oh, S. H.; Li, W.; Flytzani-Stephanopoulos, M.; Shen, M.; Goldsmith, B. R.; Yang, M. Surpassing the Single-Atom Catalytic Activity Limit through Paired Pt-O-Pt Ensemble Built from Isolated Pt1 Atoms. *Nat Commun* **2019**, *10* (1), 3808. https://doi.org/10.1038/s41467-019-11856-9.

(7) Lu, Y.; Thompson, C.; Kunwar, D.; Datye, A. K.; Karim, A. M. Origin of the High CO Oxidation Activity on CeO2 Supported Pt Nanoparticles: Weaker Binding of CO or Facile Oxygen Transfer from the Support? *ChemCatChem* **2020**, *12* (6), 1726–1733. https://doi.org/10.1002/cctc.201901848.

(8) An, K.; Alayoglu, S.; Musselwhite, N.; Plamthottam, S.; Melaet, G.; Lindeman, A. E.; Somorjai, G. A. Enhanced CO Oxidation Rates at the Interface of Mesoporous Oxides and Pt Nanoparticles. *J Am Chem Soc* **2013**, *135* (44), 16689–16696. https://doi.org/10.1021/ja4088743.

(9) van Spronsen, M. A.; Frenken, J. W. M.; Groot, I. M. N. Surface Science under Reaction Conditions: CO Oxidation on Pt and Pd Model Catalysts. *Chem Soc Rev* **2017**, *46* (14), 4347–4374. https://doi.org/10.1039/C7CS00045F.

(10) Montini, T.; Melchionna, M.; Monai, M.; Fornasiero, P. Fundamentals and Catalytic Applications of CeO2 -Based Materials. *Chem Rev* **2016**, *116* (10), 5987–6041. https://doi.org/10.1021/acs.chemrev.5b00603.

(11) Nie, L.; Mei, D.; Xiong, H.; Peng, B.; Ren, Z.; Hernandez, X. I. P.; DeLaRiva, A.; Wang, M.; Engelhard, M. H.; Kovarik, L.; Datye, A. K.; Wang, Y. Activation of Surface Lattice Oxygen in Single-Atom Pt/CeO2 for Low-Temperature CO Oxidation. *Science (1979)* **2017**, *358* (6369), 1419–1423. https://doi.org/10.1126/science.aao2109.

(12) Maurer, F.; Jelic, J.; Wang, J.; Gänzler, A.; Dolcet, P.; Wöll, C.; Wang, Y.; Studt, F.; Casapu, M.; Grunwaldt, J.-D. Tracking the Formation, Fate and Consequence for

Catalytic Activity of Pt Single Sites on CeO2. *Nat Catal* **2020**, *3* (10), 824–833. https://doi.org/10.1038/s41929-020-00508-7.

(13) Zhang, Z.; Tian, J.; Lu, Y.; Yang, S.; Jiang, D.; Huang, W.; Li, Y.; Hong, J.; Hoffman, A. S.; Bare, S. R.; Engelhard, M. H.; Datye, A. K.; Wang, Y. Memory-Dictated Dynamics of Single-Atom Pt on CeO2 for CO Oxidation. *Nat Commun* **2023**, *14* (1), 2664. https://doi.org/10.1038/s41467-023-37776-3.

(14) Serna, P.; Gates, B. C. Molecular Metal Catalysts on Supports: Organometallic Chemistry Meets Surface Science. *Acc Chem Res* **2014**, *47* (8), 2612–2620. https://doi.org/10.1021/ar500170k.

(15) Zhang, Z.; Tian, J.; Lu, Y.; Yang, S.; Jiang, D.; Huang, W.; Li, Y.; Hong, J.; Hoffman, A. S.; Bare, S. R.; Engelhard, M. H.; Datye, A. K.; Wang, Y. Memory-Dictated Dynamics of Single-Atom Pt on CeO2 for CO Oxidation. *Nat Commun* **2023**, *14* (1), 2664. https://doi.org/10.1038/s41467-023-37776-3.

(16) Moliner, M.; Gabay, J. E.; Kliewer, C. E.; Carr, R. T.; Guzman, J.; Casty, G. L.; Serna, P.; Corma, A. Reversible Transformation of Pt Nanoparticles into Single Atoms inside High-Silica Chabazite Zeolite. *J Am Chem Soc* **2016**, *138* (48), 15743–15750. https://doi.org/10.1021/jacs.6b10169.

(17) Zhang, Q.; Gao, S.; Yu, J. Metal Sites in Zeolites: Synthesis, Characterization, and Catalysis. *Chem Rev* **2023**, *123* (9), 6039–6106. https://doi.org/10.1021/acs.chemrev.2c00315.

(18) Liu, L.; Corma, A. Metal Catalysts for Heterogeneous Catalysis: From Single Atoms to Nanoclusters and Nanoparticles. *Chem Rev* **2018**, *118* (10), 4981–5079. https://doi.org/10.1021/acs.chemrev.7b00776.

(19) Serna, P.; Rodríguez-Fernández, A.; Yacob, S.; Kliewer, C.; Moliner, M.; Corma, A. Single-Site vs. Cluster Catalysis in High Temperature Oxidations. *Angewandte Chemie International Edition* **2021**, *60* (29), 15954–15962. https://doi.org/10.1002/anie.202102339.

(20) Theis, J. R.; Ura, J.; Getsoian, A. B.; Prikhodko, V. Y.; Thomas, C. R.; Pihl, J. A.; Lardinois, T. M.; Gounder, R.; Wei, X.; Ji, Y.; Pace, R. B.; Crocker, M. Effect of Framework Al Pairing on NO Storage Properties of Pd-CHA Passive NOx Adsorbers. *Appl Catal B* **2023**, *322*, 122074. https://doi.org/10.1016/j.apcatb.2022.122074.

(21) Gates, B. C. Supported Metal Clusters: Synthesis, Structure, and Catalysis. *Chem Rev* **1995**, *95* (3), 511–522. https://doi.org/10.1021/cr00035a003.

(22) Moliner, M.; Gabay, J.; Kliewer, C.; Serna, P.; Corma, A. Trapping of Metal Atoms and Metal Clusters by Chabazite under Severe Redox Stress. *ACS Catal* **2018**, *8* (10), 9520–9528. https://doi.org/10.1021/acscatal.8b01717.

(23) Felvey, N.; Guo, J.; Rana, R.; Xu, L.; Bare, S. R.; Gates, B. C.; Katz, A.; Kulkarni, A. R.; Runnebaum, R. C.; Kronawitter, C. X. Interconversion of Atomically Dispersed Platinum Cations and Platinum Clusters in Zeolite ZSM-5 and Formation of Platinum Gem -Dicarbonyls. *J Am Chem Soc* **2022**, *144* (30), 13874–13887. https://doi.org/10.1021/jacs.2c05386.

(24) Dinh, K. T.; Sullivan, M. M.; Narsimhan, K.; Serna, P.; Meyer, R. J.; Dincă, M.; Román-Leshkov, Y. Continuous Partial Oxidation of Methane to Methanol Catalyzed by Diffusion-Paired Copper Dimers in Copper-Exchanged Zeolites. *J Am Chem Soc* **2019**, *141* (29), 11641–11650. https://doi.org/10.1021/jacs.9b04906.

(25) Di Iorio, J. R.; Gounder, R. Controlling the Isolation and Pairing of Aluminum in Chabazite Zeolites Using Mixtures of Organic and Inorganic Structure-Directing Agents. *Chemistry of Materials* **2016**, *28* (7), 2236–2247. https://doi.org/10.1021/acs.chemmater.6b00181.

(26) Liu, L.; Lopez-Haro, M.; Lopes, C. W.; Li, C.; Concepcion, P.; Simonelli, L.; Calvino, J. J.; Corma, A. Regioselective Generation and Reactivity Control of Subnanometric Platinum Clusters in Zeolites for High-Temperature Catalysis. *Nat Mater* **2019**, *18* (8), 866–873. https://doi.org/10.1038/s41563-019-0412-6.

(27) Liu, L.; Lopez-Haro, M.; Lopes, C. W.; Li, C.; Concepcion, P.; Simonelli, L.; Calvino, J. J.; Corma, A. Regioselective Generation and Reactivity Control of Subnanometric Platinum Clusters in Zeolites for High-Temperature Catalysis. *Nat Mater* **2019**, *18* (8), 866–873. https://doi.org/10.1038/s41563-019-0412-6.

(28) Liu, L.; Lopez-Haro, M.; Lopes, C. W.; Rojas-Buzo, S.; Concepcion, P.; Manzorro, R.; Simonelli, L.; Sattler, A.; Serna, P.; Calvino, J. J.; Corma, A. Structural Modulation and Direct Measurement of Subnanometric Bimetallic PtSn Clusters Confined in Zeolites. *Nat Catal* **2020**, *3* (8), 628–638. https://doi.org/10.1038/s41929-020-0472-7.

(29) Burton, A.; Terefenko, E.; Wang, H.; Paccagnini, M.; Sattler, A. Structure-Property Relationships That Influence Platinum Stability in All-Silica or Highly Siliceous Zeolites. *Microporous and Mesoporous Materials* **2023**, *350*, 112411. https://doi.org/10.1016/j.micromeso.2022.112411.

(30) Ramaker, D. E.; de Graaf, J.; van Veen, J. A. R.; Koningsberger, D. C. Nature of the Metal–Support Interaction in Supported Pt Catalysts: Shift in Pt Valence Orbital Energy and Charge Rearrangement. *J Catal* **2001**, *203* (1), 7–17. https://doi.org/10.1006/jcat.2001.3299.

(31) Visser, T.; Nijhuis, T. A.; van der Eerden, A. M. J.; Jenken, K.; Ji, Y.; Bras, W.; Nikitenko, S.; Ikeda, Y.; Lepage, M.; Weckhuysen, B. M. Promotion Effects in the Oxidation of CO over Zeolite-Supported Pt Nanoparticles. *J Phys Chem B* **2005**, *109* (9), 3822–3831. https://doi.org/10.1021/jp044767f.

(32) Yang, X.; Su, X.; Chen, X.; Duan, H.; Liang, B.; Liu, Q.; Liu, X.; Ren, Y.; Huang, Y.; Zhang, T. Promotion Effects of Potassium on the Activity and Selectivity of Pt/Zeolite Catalysts for Reverse Water Gas Shift Reaction. *Appl Catal B* **2017**, *216*, 95–105. https://doi.org/10.1016/j.apcatb.2017.05.067.

(33) Liu, L.; Lopez-Haro, M.; Lopes, C. W.; Rojas-Buzo, S.; Concepcion, P.; Manzorro, R.; Simonelli, L.; Sattler, A.; Serna, P.; Calvino, J. J.; Corma, A. Structural Modulation and Direct Measurement of Subnanometric Bimetallic PtSn Clusters Confined in Zeolites. *Nat Catal* **2020**, *3* (8), 628–638. https://doi.org/10.1038/s41929-020-0472-7.

(34) Authors Note That Standard Blurring Effects in Our STEM Instrument (e.g. Electron Beam Probe Size,Vibrational Instabilities, Irradiation Effects, Off-Focus, Beam Broadening, Etc.) Are Expected to Cause a Slight Overestimation of the Sizes of the Clusters, and Some Broadening of the Size Distribution, Relative to Previous Reports.

(35) Meunier, F. C. Relevance of IR Spectroscopy of Adsorbed CO for the Characterization of Heterogeneous Catalysts Containing Isolated Atoms. *Journal of Physical Chemistry C* **2021**, *125* (40), 21810–21823. https://doi.org/10.1021/acs.jpcc.1c06784.

(36) Miessner, H.; Burkhardt, I.; Gutschick, D.; Zecchina, A.; Morterra, C.; Spoto, G. The Formation of a Well Defined Rhodium Dicarbonyl in Highly Dealuminated Rhodium-Exchanged Zeolite Y by Interaction with CO. *Journal of the Chemical Society, Faraday Transactions 1: Physical Chemistry in Condensed Phases* **1989**, *85* (8), 2113. https://doi.org/10.1039/f19898502113.

(37) Bourane, A.; Dulaurent, O.; Bianchi, D. Heats of Adsorption of the Linear CO Species Adsorbed on a Pt/Al 2 O 3 Catalyst in the Presence of Coadsorbed Species Using FTIR Spectroscopy. *Langmuir* **2001**, *17* (18), 5496–5502. https://doi.org/10.1021/la0015361.

(38) Lu, J.; Serna, P.; Aydin, C.; Browning, N. D.; Gates, B. C. Supported Molecular Iridium Catalysts: Resolving Effects of Metal Nuclearity and Supports as Ligands. *J Am Chem Soc* **2011**, *133* (40), 16186–16195. https://doi.org/10.1021/ja206486j.

(39) Goodman, E. D.; Johnston-Peck, A. C.; Dietze, E. M.; Wrasman, C. J.; Hoffman, A. S.; Abild-Pedersen, F.; Bare, S. R.; Plessow, P. N.; Cargnello, M. Catalyst Deactivation via Decomposition into Single Atoms and the Role of Metal Loading. *Nat Catal* **2019**, *2* (9), 748–755. https://doi.org/10.1038/s41929-019-0328-1.

(40) Neumann, S.; Gutmann, T.; Buntkowsky, G.; Paul, S.; Thiele, G.; Sievers, H.; Bäumer, M.; Kunz, S. Insights into the Reaction Mechanism and Particle Size Effects of CO Oxidation over Supported Pt Nanoparticle Catalysts. *J Catal* **2019**, *377*, 662–672. https://doi.org/10.1016/j.jcat.2019.07.049.

(41) The Uncertainty of This Particle Size Distribution and Average Particle Size Is Greater than in Other Sample with Slightly Larger Pt Clusters, Because of Detection Limitation under Our Microscope.

(42) Silaghi, M.-C.; Chizallet, C.; Raybaud, P. Challenges on Molecular Aspects of Dealumination and Desilication of Zeolites. *Microporous and Mesoporous Materials* **2014**, *191*, 82–96. https://doi.org/10.1016/j.micromeso.2014.02.040.

Associated content

Characterization of the materials including ICP-OES analysis, X Ray Diffraction patterns, BET isotherms, FESEM and TEM images before and after catalysis and 50ROR cycles,

comparison of the catalytic performance with different Pt particles sizes and catalytic performance of the materials after 50ROR cycles.